Three Polymeric Frameworks Constructed from Discrete Molybdenum Oxide Anions and 4,4′-bpy-Bridged Linear Polymeric Copper Cations

Can-Zhong Lu,* Chuan-De Wu, Hong-Hui Zhuang, and Jin-Shun Huang

The State Key Laboratory of Structural Chemistry, Fujian Institute of Research on the Structure of Matter, Chinese Academy of Sciences, Fuzhou, Fujian 350002, P.R. China

Received December 20, 2001

Three compounds, $[Cu(4,4'\text{-bpy})]_2MoO_4\cdot 2H_2O$ (**1**), $[Cu(4,4'\text{-bpy})]_2Mo_2O_7$ (**2**), and $[Cu(4,4'\text{-bpy})(nic)(H_2O)]_2Mo_8O_{26}$ (**3**), are synthesized by hydrothermal reaction, which suggests that oxomolybdate−organic ligand coordination transition-metal fragments can merge their merit to generate some interesting architectures. Crystal data for $[Cu(4,4'\text{-bpy})]_2MoO_4\cdot 2H_2O$ (**1**): monoclinic system, space group $C2/c$, $a = 10.936(1)$, $b = 17.775(1)$, and $c = 14.484(1)$ Å, $\beta = 110.15(1)°$, and $Z = 4$. Crystal data for $[Cu(4,4'\text{-bpy})]_2Mo_2O_7$ (**2**): orthorhombic system, space group $Pbcn$, $a = 11.841(1)$, $b = 9.105(1)$, and $c = 21.311(1)$ Å, and $Z = 4$. Crystal data for $[Cu(4,4'\text{-bpy})(nic)(H_2O)]_2Mo_8O_{26}$ (**3**): monoclinic system, space group $P2(1)/n$, $a = 11.457(1)$, $b = 16.918(1)$, and $c = 12.463(1)$ Å, $\beta = 92.6(1)°$, and $Z = 2$. Compound **1** is built up from $\{MoO_4\}$ tetrahedra linking of 4,4′-bpy coordination copper(I) chain fragments as a railroad-like framework. Compound **2** has noticeable structural features: two $\{Mo_2O_7\}$ and four $\{CuO_2N_2\}$ tetrahedra are connected to each other alternately in a pattern of corner sharing to construct an eight-metal-central-membered cavity; such subunits are connected to each other also through corner-shared, two-dimensional mosaic frameworks, which are linked further by bidentate 4,4′-bpy ligands to a three-dimensional framework with oval channels. The two-dimensional flat brick wall-like layer structure of **3** is constructed from two layer $[Cu(4,4'\text{-bpy})(nic)(H_2O)]_n^{2n+}$ chains joined together by β-$[Mo_8O_{26}]^{4-}$ units as tethers through covalent bonding of the terminal oxo groups to form rectangular cavities. The most curious feature of **3**, however, is that the extended structure of **3** is comprised of an interpenetrated arrangement of two kinds of multizigzag chain polymers entangled together. The successful assembly of the three polymeric frameworks of **1**−**3** demonstrates the dramatic influence of the reaction acidity/basicity on the organization of molecular building groups and further on the construction of solid architectures. The studies of the temperature dependence of the magnetic susceptibilities of **3** reveal that there exists the weak magnetic transformation of 4,4′-bpy and octamolybdate between metal ions.

1. Introduction

Metal oxide based solids, especially heteropolyoxometalates, have provoked significant contemporary interest. Over the past few years, considerable researches have been directed at the preparation of metal oxide based solids, partly because of interest in chemistry itself and also because of interest in their applications.[1−7] Despite the fact that rational design techniques and methods are continuing at an accelerating development stage,[8] one is not able to adequately rationalize the synthesis of a variety of open-framework polymers, and the "rational" design of reliable synthetic strategies in polymetallic compounds is still the major challenge facing chemists.[9]

* To whom correspondence should be addressed. E-mail: czlu@ms.fjirsm.ac.cn.

(1) Cheetham, A. K. *Science* **1994**, *264*, 794 and references therein.
(2) Müller, A.; Reuter, H.; Dillinger, S. *Angew. Chem., Int. Ed. Engl.* **1995**, *34*, 2328.
(3) Pope, M. T.; Müller, A. *Angew. Chem., Int. Ed. Engl.* **1991**, *30*, 34.
(4) Cox, P. A. *Transition Metal Oxides*; Clarendon Press: Oxford, England, 1995.
(5) Pope, M. T. *Heteropoly and Isopoly Oxometalates*; Springer: New York, 1983. Pope, M. T.; Müller, A. *Polyoxometalates: From Platonic Solids to Anti-Retroviral Activety*; Kluwer Academic: Dordrecht, The Netherlands, 1994.
(6) Müller, A.; Peters, F.; Pope, M. T.; Gatteschi, D. *Chem. Rev.* **1998**, *98*, 239.
(7) (a) Yaghi, O. M.; Li, H.; Davis, C.; Richardson, D.; Groy, T. L. *Acc. Chem. Res.* **1998**, *31*, 474. Yaghi, O. M. *Nature* **1999**, 402, 276. (b) Yaghi, O. M.; Li, H. *J. Am. Chem. Soc.* **1996**, *118*, 295. Yaghi, O. M. *J. Am. Chem. Soc.* **1998**, *120*, 8571.
(8) For example, (a) Wolff, J. J. *Angew. Chem., Int. Ed. Engl.* **1996**, *35*, 2195. (b) Davis, M. E. *Chem. Eur. J.* **1997**, *3*, 1745. (c) *Crystal Engineering: the Design of Organic Solids*; Materials Science Monographs 54; Elsevier: Amsterdam, The Netherlands, 1989.
(9) (a) Maddox, J. S. *Nature* **1988**, *335*, 201. (b) Gavezzotti, A. *Acc. Chem. Res.* **1994**, *27*, 309. (c) Zaworotko, M. J. *Angew. Chem., Int. Ed.* **2000**, *39*, 3052. (d) Caneschi, A.; Cornia, A.; Fabretti, A. C.; Gatteschi, D. *Angew. Chem., Int. Ed. Engl.* **1995**, *34*, 2716. (e) DiSalvo, F. J. *Science* **1990**, *247*, 649. (f) Squire, R. C.; Aubin, S. M. J.; Folting, K.; Streib, W. E.; Hendrickson, D. N.; Christou, G. *Angew. Chem., Int. Ed. Engl.* **1995**, *34*, 887. (g) Powell, A. K.; Heath, S. L.; Gatteschi, D.; Pardi, L.; Sessoli, R.; Spina, G.; Giollo, F.-D.; Pieralli, F. *J. Am. Chem. Soc.* **1995**, *117*, 2491. (h) Braga, D.; Grepioni, F.; Orpen, A. G. *Crystal Engineering: From Molecules and Crystals to Materials*; NATO Science Series; Kluwer Academic Publishers: Dordrecht, The Netherlands, 1999. (i) Caneschi, A.; Cornia, A.; Fabretti A. C.; Gatteschi, D. *Angew. Chem., Int. Ed. Engl.* **1995**, *34*, 2716.

10.1021/cm011725k CCC: $22.00
Published on Web 04/30/2002

Recent elaboration has proven that hydrothermal reaction at relatively low temperature (110−260°) and pressure, which causes a reaction shift from the kinetic to the thermodynamic domain compared to traditional aqueous reactions, such that the equilibrium phases are replaced by more complex metastable phases,[10] provides a powerful tool for the introduction of organic ligands into oxide structures. Molybdenum in its high oxidation state with higher reacting ability tends to form mononuclear, polynuclear anionic metal−oxygen clusters or oligomers, such as $\{Mo_2O_7\}$, $\{Mo_3O_{10}\}$, $\{Mo_6O_{19}\}$, $\{Mo_8O_{26}\}$, etc., and a second transition-metal center (e.g., Mn, Fe, Co, Ni, Cu, and Zn) will provide distinct geometric biases to form metal−organic coordination fragments with various metal cation/donor atom interactions, which provides significant structural flexibility. One of the crucial strategies for the molecular design of solid materials is how to employ a hydrothermal synthesis method to introduce some interesting transition-metal-coordinated complexes, which usually serve as organic−inorganic bridging ligands, into the covalent backbone of solid materials. Normally, such transition-metal complexes act as a covalent linker to molybdate, either as monomeric $[MoO_4]^{2-}$ or as oligomeric $[Mo_xO_y]^{n-}$, or as one- or two-dimensional networks and are considered as charge-balancing anions for the cationic coordination polymers, to extend novel products into higher dimensional frameworks.[11] So far, a wide range of novel heterooxometalates existing as molybdenum oxides with second mononuclear, binuclear, and trinuclear metal centers have been reported.[12] Because of the ability of transition-metal elements to adapt various coordination geometries in different oxidation states, the influences of second metal ions as well as organic ligands on the structural types could be studied by modifying transition-metal ions, organic groups, and synthetic conditions.

So, the combination of these two aspects of molybdenum oxides and metal−organic coordination fragments with their significant structural features might merge their merit to generate some interesting compounds with special properties. We have launched a systematic program aimed at linking some mono- or polyoxometalate building groups by organic ligand coordinated transition-metal fragments to generate some distinctive architectures. By hydrothermal reactions, we report here the syntheses, structural characterization, and physical properties of three architectures with one-, two-, and three-dimensional frameworks: $[Cu(4,4'\text{-bpy})]_2MoO_4{\cdot}2H_2O$ (**1**), $[Cu(4,4'\text{-bpy})]_2Mo_2O_7$ (**2**), and $[Cu(4,4\text{-bipy})(nic)(H_2O)]_2Mo_8O_{26}$ (**3**).

(10) (a) Gopalakrishnan, J. *Chem. Mater.* **1975**, *7*, 1265. (b) Rabenau, A. *Angew. Chem., Int. Ed. Engl.* **1985**, *24*, 1026. (c) Ludise, R. A. *Chem. Eng. News* **1987**, *65* (40), 30. (d) Lu, J. Y.; Lawandy, M. L.; Li, J.; Yuen, T.; Lin, C. L. *Inorg. Chem.* **1999**, *38*, 2695.

(11) (a) Bu, W.-M.; Yang, G.-Y.; Ye, L.; Xu, J.-Q.; Fan, Y.-G. *Chem. Lett.* **2000**, 462. (b) Xu, J.-Q.; Wang, R.-Z.; Yang, G.-Y.; Xing, Y.-H.; Li, D.-L.; Bu, W.-M.; Ye, L.; Fan, Y.-G.; Yang, G.-D.; Xing, Y.; Lin, Y.-H.; Jia, H.-Q. *Chem. Commun.* **1999**, 983. (c) Xu, J. J.; Xu, Y.; Goh, N. K.; Chia, L. S. *Chem. Commun.* **1998**, 1709. (d) Hagrman, D.; Zapf, P. J.; Zubieta, J. *Chem. Commun.* **1998**, 1283. (e) Hagrman, D.; Zubieta, J. *Chem. Commun.* **1998**, 2005. (f) LaDuca, R. L., Jr.; Finn, R.; Zubieta, J. *Chem. Commun.* **1999**, 1669.

(12) (a) Hagrman, P. J.; Hagrman, D.; Zubieta, J. *Angew. Chem., Int. Ed.* **1999**, *38*, 2638 and references therein. (b) Chesnut, D. J.; Hagrman, D.; Zapf, P. J.; Hammond, R. P., Jr.; Haushalter, R. C.; Zubieta, J. *Coord. Chem. Rev.* **1999**, *190*−*192*, 737 and references therein. (c) Huang, S. D.; Shan, Y. *J. Solid State Chem.* **2000**, *152*, 229. (d) Hagrman, D. E.; Zubieta, J. *J. Solid State Chem.* **2000**, *152*, 141. (e) LaDuca, R. L., Jr.; Desciak, M.; Laskoski, M.; Rarig, R. S., Jr.; Zubieta, J. *J. Chem. Soc., Dalton Trans.* **2000**, 2255.

2. Experimental Section

2.1. Materials and Methods. All chemicals were of reagent grade and were used as received from commercial sources without further purification. Element analyses were performed via a Vario EL III CHNOS element analyzer. Infrared spectra were recorded on a FTS-40 spectrophotometer by use of pressed KBr pellets. The FT−Raman spectra were measured on a Nicolet Raman 910 Fourier transform laser−Raman spectrum by use of pressed KBr pellets, and electron spin resonance (ESR) was performed on a Bruker ER 420 model. Variable-temperature magnetic susceptibilities were measured on a model CF-1 superconducting extracting sample magnetometer with a powder sample kept in a capsule for weighing. All data were corrected for diamagnetism of the ligands estimated from Pascal's constants.[13]

2.2. Syntheses. The syntheses were performed in sealed 30 mL Teflon-lined stainless steel vessels.

1. A mixture of $Na_2MoO_4{\cdot}H_2O$ (0.10 g, 0.41 mmol), $CuSO_4{\cdot}5H_2O$ (0.10 g, 0.40 mmol), 4,4′-bpy·$2H_2O$ (0.05 g, 0.26 mmol), and $NH_3{\cdot}H_2O$ (0.10 mL, 1.3 mmol) in H_2O (18 mL) was heated at 170 °C for 6 days under autogenous pressure. Brown crystals were isolated after the reaction solution was cooled gradually and washed with water and ethanol. Yield: about 46.8%, based on Mo. Anal. Calcd for **1**: C, 37.80; H, 3.17; N, 8.82. Found: C, 37.62; H, 3.31; N, 8.76. IR (solid KBr pellet, ν/cm^{-1}): 1601s, 1527s, 1483s, 1417sh, 1408s, 1371m, 1215s, 1070m, 1063sh, 818s, 798s, 723m, 642m, 476m. FT-Raman (solid, λ = 1064 nm, ν/cm^{-1}): 1606vs, 1294s, 1232s, 1082m, 1020s, 978m, 823m, 777m, 658m, 569m, 449s, 372s. Compound **1** is ESR silent at room temperature and 77 K, which is consistent with the Cu^I oxidation state.

2. A mixture of H_2MoO_4 (0.10 g, 0.62 mmol), $CuSO_4{\cdot}5H_2O$ (0.10 g, 0.40 mmol), and 4,4′-bpy·$2H_2O$ (0.05 g, 0.26 mmol) in H_2O (18 mL) was heated at 170 °C for 6 days under autogenous pressure. After the reaction was slowly cooled to room temperature, brown crystals were produced. Yield: 67.3%, based on Cu. Anal. Calcd for **2:** C, 32.32; H, 2.17; N, 7.54. Found: C, 32.28; H, 2.19; N, 7.46. IR (solid KBr pellet, ν/cm^{-1}): 1605s, 1531m, 1489m, 1419s, 1321w, 1219m, 1072w, 924m, 897s, 883sh, 864sh, 856s, 816m, 798s, 746sh, 731m, 646m, 577m, 505s. FT-Raman (solid, λ = 1064 nm, ν/cm^{-1}): 1608vs, 1295s, 1230s, 1074m, 1031s, 1020s, 921s, 885w, 867w, 813w, 798w, 777w, 476m, 449m, 381m, 327w, 179sh, 161s, 144s. Compound **2** is ESR silent at room temperature and 77 K, which is consistent with the Cu^I oxidation state.

3. The pH of a mixture of $Na_2MoO_4{\cdot}2H_2O$ (0.25 g, 1.0 mmol), $CuSO_4{\cdot}5H_2O$ (0.25 g, 1.0 mmol), 4,4′-bpy·$2H_2O$ (0.05 g, 0.26 mmol), and nicotinic acid (0.13 g, 1.1 mmol) in H_2O (18 mL) was adjusted to 2.44 and then the mixture was heated at 170 °C for 2 days under autogenous pressure. Blue crystals were isolated after the reaction solution was cooled gradually and washed with water and ethanol. Yield: 36.5%, based on Mo. Anal. Calcd for **3**: C, 20.17; H, 1.59; N, 4.41; Found: C, 20.09; H, 1.60; N, 4.38. IR (solid KBr pellet, ν/cm^{-1}): 1639m, 1612s, 1529m, 1493m, 1464m, 1421m, 1387s, 1221m, 1184w, 1161w, 1109w, 1072m, 1016w, 958s, 953s, 931m, 914m, 895s, 841m, 829m, 804m, 719s, 677s, 661s, 577sh, 563m, 525m, 480m, 459m. FT−Raman (solid, λ = 1064 nm, ν/cm^{-1}): 1621vs, 1521m, 1384m, 1290vs, 1241m, 1085m, 1037s, 967vs, 948m, 927m, 917s, 894s, 840m, 784m, 655m, 568m, 360m, 254w, 215s, 142s, 123m.

2.2. X-ray Structure Determination. The determination of the unit cell and the data collection for brown crystals of compounds **1** and **2** and blue crystals of **3** were performed on a Siemens SMART CCD, and all of the data were collected using graphite-monochromated Mo Kα radiation (λ = 0.710 73

(13) Pascal, P. *Ann. Chim. Phys.* **1910**, *19*, 5.

Table 1. Crystal Data and Structural Refinements for $[Cu(4,4'\text{-bpy})]_2MoO_4\cdot 2H_2O$ (1), $[Cu(4,4\text{-bipy})]_2Mo_2O_7$ (2), and $[Cu(4,4\text{-bipy})(nic)(H_2O)]_2Mo_8O_{26}$ (3)

compound	**1**	**2**	**3**
formula	$C_{20}H_{20}Cu_2MoN_4O_6$	$C_{20}H_{16}Cu_2Mo_2N_4O_7$	$C_{32}H_{30}Cu_2Mo_8N_6O_{32}$
formula weight	635.42	743.33	1905.22
crystal size (mm^3)	0.44 × 0.13 × 0.12	0.48 × 0.14 × 0.10	0.20 × 0.16 × 0.14
crystal color	brown	brown	blue
crystal system	monoclinic	orthorhombic	monoclinic
space group	*C*2/*c*	*Pbcn*	*P*2(1)/*n*
unit cell dimensions	$a = 10.936(1)$ Å, $\alpha = 90°$	$a = 11.841(1)$ Å	$a = 11.457(1)$ Å, $\alpha = 90°$
	$b = 17.775(1)$ Å, $\beta = 110.2(1)°$	$b = 9.105(1)$ Å	$b = 16.918(1)$ Å, $\beta = 92.6(1)°$
	$c = 14.484(1)$ Å, $\gamma = 90°$	$c = 21.311(1)$ Å	$c = 12.4634(1)$ Å, $\gamma = 90°$
volume ($Å^3$)	2643.2(2)	2297.6(1)	2413.3(1)
Z	4	4	2
calculated density ($g\cdot cm^{-3}$)	1.597	2.149	2.622
F(000)	1264	1448	1828
absorption coefficient (mm^{-1})	2.100	2.943	2.976
θ for data collection (deg)	2.29−24.00	1.91−25.10	2.03−25.05
reflections collected	4245	7826	8112
unique reflections (*R*(int))	2069 [*R*(int) = 0.0699]	2036 [*R*(int) = 0.0433]	4213 [*R*(int) = 0.0230]
data/restraints/parameters	2069/0/169	2036/0/160	4213/0/418
goodness of fit on F^2	1.038	1.103	1.085
final *R* indices [$I > 2\sigma(I)$][a]	R1 = 0.0807, wR2 = 0.2141	R1 = 0.0362, wR2 = 0.0848	R1 = 0.0305, wR2 = 0.0654
R indices (all data)	R1 = 0.1258, wR2 = 0.2326	R1 = 0.0567, wR2 = 0.0959	R1 = 0.0428, wR2 = 0.0715
largest diff. peak and hole ($e\cdot Å^3$)	+1.148 and −0.845	+0.769 and −0.845	+1.055 and −0.634

[a] $R1 = \sum(|F_o| - |F_c|)/\sum|F_o|$. $wR2 = [\sum w(F_o^2 - F_c^2)^2/\sum w(F_o^2)^2]^{0.5}$.

Table 2. Selected Bond Lengths (Å) and Angles (deg) for 1−3[a]

		Complex **1**			
Mo(1)−O(2)	1.746(8)	O(2)^{i}−Mo(1)−O(2)	109.8(7)	N(1)−Cu(1)−N(2)	161.1(4)
Mo(1)−O(1)	1.756(10)	O(2)^{i}−Mo(1)−O(1)	109.6(4)	N(1)−Cu(1)−O(1)	100.1(3)
Cu(1)−N(1)	1.907(8)	O(2)^{i}−Mo(1)−O(1)^{i}	109.2(5)	N(2)−Cu(1)−O(1)	98.5(3)
Cu(1)−N(2)	1.918(8)	O(1)−Mo(1)−O(1)^{i}	109.5(7)	Mo(1)−O(1)−Cu(1)	132.2(6)
Cu(1)−O(1)	2.212(9)				
		Complex **2**			
Mo(1)−O(2)	1.699(5)	O(2)−Mo(1)−O(3)	109.2(2)	N(2)−Cu(1)−O(4)	103.1(2)
Mo(1)−O(3)	1.715(3)	O(2)−Mo(1)−O(4)	108.7(2)	N(1)^{ii}−Cu(1)−O(4)	100.7(2)
Mo(1)−O(4)	1.719(3)	O(3)−Mo(1)−O(4)	110.1(2)	N(2)−Cu(1)−O(3)^{iii}	91.4(1)
Mo(1)−O(1)	1.867(1)	O(2)−Mo(1)−O(1)	109.7(2)	N(1)^{ii}−Cu(1)−O(3)^{iii}	100.4(1)
Cu(1)−N(2)	1.924(4)	O(3)−Mo(1)−O(1)	109.1(2)	O(4)−Cu(1)−O(3)^{iii}	91.6(1)
Cu(1)−N(1)^{ii}	1.933(4)	O(4)−Mo(1)−O(1)	110.0(2)	Mo(1)−O(1)−Mo(1)^{iv}	167.2(4)
Cu(1)−O(4)	2.201(4)	N(2)−Cu(1)−N(1)^{ii}	153.1(2)	Mo(1)−O(4)−Cu(1)	159.0(2)
Cu(1)−O(3)^{iii}	2.590(4)				
		Complex **3**			
Cu(1)−O(1)	1.930(5)	O(1)−Cu(1)−O(13)	88.0(2)	O(1)−Cu(1)−O(16)	98.8(2)
Cu(1)−O(13)	1.958(3)	O(1)−Cu(1)−N(2)	89.2(2)	O(13)−Cu(1)−O(16)	92.0(2)
Cu(1)−N(2)	1.995(4)	O(13)−Cu(1)−N(2)	172.2(2)	N(2)−Cu(1)−O(16)	95.6(2)
Cu(1)−N(3)	1.995(4)	O(1)−Cu(1)−N(3)	167.9(3)	N(3)−Cu(1)−O(16)	92.6(2)
Cu(1)−O(16)	2.276(4)	O(13)−Cu(1)−N(3)	87.7(2)	Mo(3)−O(16)−Cu(1)	136.0(2)
		N(2)−Cu(1)−N(3)	93.7(2)		

[a] Symmetry transformations used to generate equivalent atoms: i, $-x, y, -z + 1/2$; ii, $x, -y, z - 1/2$; iii, $-x - 3/2, y + 1/2, z$; iv, $-x - 1, y, -z - 1/2$.

Å) at 293 K. The data sets were corrected by the SADABS program.[14] The structures were solved by direct methods and refined by full-matrix least-squares methods. The structural solutions and refinement were carried out using the SHELXL-97 software package.[15] All atoms except hydrogen atoms were refined anisotropically. The oxidation state bound value of copper atoms in **1** and **2** can be unambiguously assigned as +1 on the basis of charge neutrality, the crystal color, the coordination environments, and the ESR spectra, which may be reduced by the 4,4′-bpy ligand and are similar to previous publications.[16] Crystallographic data are summarized in Table 1 and the selected bond lengths and angles in Table 2.

3. Results and Discussion

3.1. Syntheses and Structures. It has been well-known that the forming of different oxomolybdate phases is mainly controlled by the pH values, which suggests that careful control of the reaction acidity/basicity can gain different building groups. Under basified reaction conditions (pH > 7), mononuclear molybdate $\{MoO_4\}$ tends to form. Increasing the reaction acidity to pH < 7 readily induces the polyoxomolybdate, such as $\{Mo_2O_7\}$, $\{Mo_3O_{10}\}$, $\{Mo_6O_{19}\}$, $\{Mo_8O_{26}\}$, etc., to form. This observation has been well-known in the aqueous molybdate (Mo^{VI}) chemistry, where the concentration of $\{MoO_x\}$ polyhedra is fixed via increasing reaction acidity. Also, the different acidity/basicity values of the reaction under hydrothermal reaction media might also influence the transformation of different oxidation states of second transition-metal elements, such as copper elements (I or II). In a systematic

(14) Sheldrick, G. M. *SADABS*; Siemens Analytical X-ray Instrument Division: Madison, WI, 1995.

(15) Sheldrick, G. M. Universität Göttingen, Germany, 1997.

(16) (a) Hagrman, D.; Hagrman, P.; Zubieta, J. *Inorg. Chem. Acta* **2000**, *300*, 212. You, W.-S.; Wang, E.-B.; Xu, L.; Hu, C.-W.; Luan, G.-Y. *Acta Crystallogr.* **2000**, *C56*, 289. (b) Hagrman, D.; Zubieta, C.; Rose, D. J.; Zubieta, J.; Haushalter R. C. *Angew. Chem., Int. Ed. Engl.* **1997**, *36*, 873. (c) Hagrman, D.; Zapf, P. J.; Zubieta, J. *Chem. Commun.* **1998**, 1283. (d) Hagrman, D.; Zubieta, J. *Chem. Commun.* **1998**, 2005.

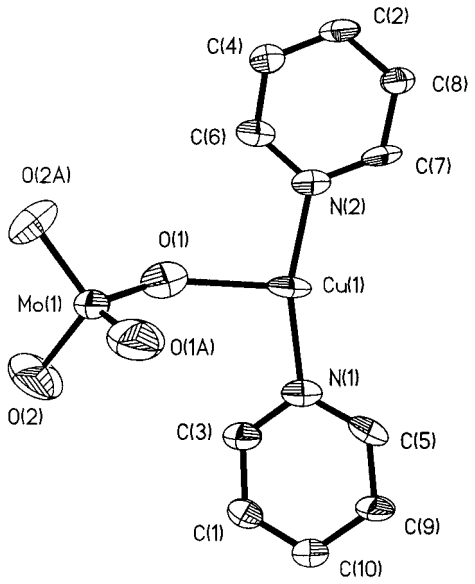

Figure 1. ORTEP representation of the symmetry-expanded local structure for **1** (50% probability ellipsoids).

study of the impact of the pH values under the hydrothermal reaction media on the formation of of hybrid materials, we employed molybdate, copper(II) salt, and 4,4′-bpy ligand at various acidity/basicity values in an assembly of novel extended solid materials containing molybdenum(VI) mono- and polyoxoanions and 4,4′-bpy coordination copper fragments. Successful isolations of one-dimensional $[Cu(4,4'\text{-bpy})]_2MoO_4{\cdot}2H_2O$ (**1**), three-dimensional $[Cu(4,4'\text{-bpy})]_2Mo_2O_7$ (**2**), and two-dimensional $[Cu(4,4'\text{-bpy})(nic)(H_2O)]_2Mo_8O_{26}$ (**3**) once again demonstrate the crucial role of the reaction acidity/basicity in the construction of hybrid materials, especially copper−organic−molybdate materials.

The hydrothermal reaction of $Na_2MoO_4{\cdot}2H_2O$, $CuSO_4{\cdot}5H_2O$, 4,4′-bpy, and water gave rise to **1** as brown crystals under weak basified conditions. The IR spectrum of **1** exhibits strong bands at 818 and 798 cm^{-1}, which are attributed to ν(Mo═O), and bands in the 1601−1215 cm^{-1} range, which are for the 4,4′-bpy ligand. The Raman spectra at 1606, 1294, 1232, 1082, and 1020 cm^{-1} are ascribed to the 4,4′-bpy ligand and those at 978, 823, and 777 cm^{-1} to ν(Mo═O). Single-crystal structure analysis has revealed that compound **1** contains a one-dimensional railroad-like linear framework. As shown in Figure 1, each copper(I) atom is three-coordinated trigonal, which is coordinated by two nitrogen atoms from two 4,4′-bpy ligands (Cu−N = 1.907(8) and 1.918(8) Å) and one oxygen atom from a $\{MoO_4\}$ tetrahedron (Cu−O = 2.213(9) Å), with O(N)−Cu−O(N) angles ranging from 98.5(3) to 161.1(4)°. In this way, each 4,4′-bpy ligand links two symmetry-related copper(I) atoms into a one-dimensional chain. The most interesting feature of **1** is that these chains are further linked by $\{MoO_4\}$ tetrahedra, acting as inorganic ligands, up and down these chains to form a novel infinite linear railroad-like framework (Figure 2).

The hydrothermal reaction of H_2MoO_4, $CuSO_4{\cdot}5H_2O$, 4,4′-bpy, and water gave rise to **2** as brown crystals under weak acidic conditions. The IR spectrum of **2** exhibits multiple bands in the 1605−1072 cm^{-1} range, attributed to the 4,4′-bpy ligand absorption. The bands in the range 924−731 cm^{-1} are ascribed to ν(Mo═O) and

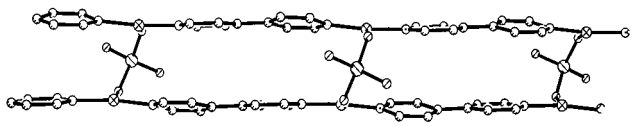

Figure 2. View of the extended **1**, showing the railroad-like structure.

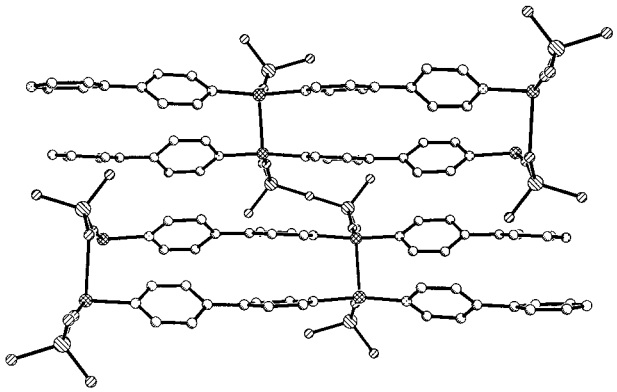

Figure 3. Viewed down the *b* axis for **2**, showing the linkage between $[Mo_2O_7]^{2-}$ anions and $[Cu(4,4'\text{-bpy})]_n^{n+}$ (Mo, large left-hatched; Cu, cross-hatched; O, small right-hatched; C, shaded).

ν(Mo−O−Mo). Similarly, the Raman spectrum also exhibits several bands in the range of 1608−1020 and 921−777 cm^{-1} for the 4,4′-bpy ligand and ν(Mo═O) or ν(Mo−O−Mo), respectively. Single-crystal structure analysis shows that the structure and cell parameters of **2** are almost similar to those in previous publications.[16a] Because there are so many structural features that have not been discovered, it is still worth describing here. It is composed of one-dimensional $[Cu(4,4'\text{-bpy})]_n^{n+}$ polymers linked by $[Mo_2O_7]^{2-}$ subunits to generate a three-dimensional framework with interesting features. The structure can also be described as a layer $\{Cu_2Mo_2O_7\}$ metal oxide network linked by organic ligands into a three-dimensional network.

As shown in Figure 3, the Cu^I coordination geometry is defined by two nitrogen donors from two 4,4′-bpy ligands and two oxygen donors from two adjacent $[Mo_2O_7]^{2-}$ cluster anions with Cu−O bond lengths of 2.201(4) and 2.590(4) Å, respectively. The later Cu−O bond length is quite long, indicating a weak long-range interaction of copper(I) with the oxygen atom, which is similar to previous publications.[16,17] Each 4,4′-bpy ligand bridges two neighboring Cu^I sites, so that each $[Cu(4,4'\text{-bpy})_4]^+$ group links to two adjacent Cu^I centers to give a linear chain. Two adjacent Cu^I centers are separated by 4,4′-bpy ligands by about 10.938 Å. The dimolybdate subunit, built up by two corner-shared $\{MoO_4\}$ tetrahedra, is employed as an effective tether through four terminal oxo groups of the cluster to link four adjacent $[Cu(4,4'\text{-bpy})_4]_n^{n+}$ groups into a three-dimensional framework.

With the omission of the organic ligands and viewed parallel to the [001] plane, compound **2** has a remarkable bimetallic two-dimensional $\{Cu_2Mo_2\}$ inorganic backbone network (Figure 4a), which might also be described as a bilayer of corner-sharing $\{MoO_4\}$ and

(17) DeRord, J. R. D.; Haushalter, R. C.; Meyer, L. M.; Rose, D. J.; Zapf, P. J.; Zubieta, J. *Inorg. Chem. Acta* **1997**, *256*, 165.

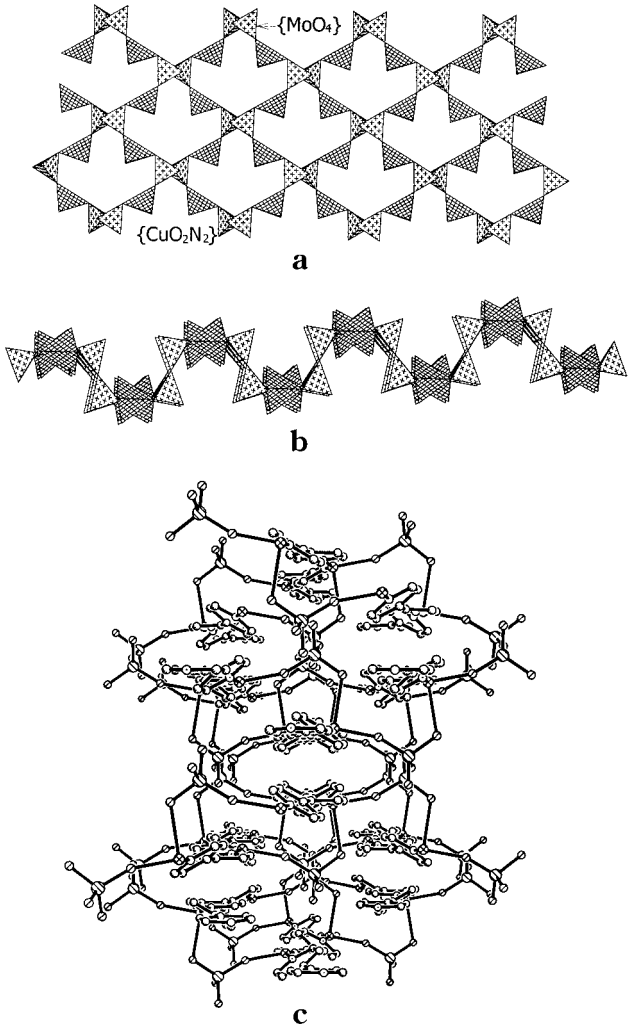

Figure 4. (a) Polyhedral representation of the $\{Cu_2Mo_2\}$ layer and the environments of $\{MoO_4\}$ and $\{CuO_2N_2\}$ tetrahedra, showing the mosaic structure of **2**. (b) View of the substructure $\{Cu_2Mo_2\}$ of **2** along the crystallographic *b* axis (with omission of organic ligands), showing a zigzag chain parallel to the *a* axis. (c) Viewed down the *c* axis, showing the channels of **2**.

$\{CuO_2N_2\}$ tetrahedra. Interestingly, a view of the substructure $\{Cu_2Mo_2\}$ of **2** along the crystallographic *b* axis shows a zigzag chain (Figure 4b). It is most noticeable that four $\{MoO_4\}$ and four $\{CuO_2N_2\}$ tetrahedra are connected to each other alternatively in a pattern of corner sharing to construct an eight-metal-central-membered ring with a dimension of about 5.497 × 9.105 Å. Then, such rings are linked by $\{MoO_4\}$ tetrahedra via corner sharing into a unique two-dimensional open framework. Finally, the bimetallic $\{Cu_2Mo_2\}$ layers are linked by bidentate 4,4′-bpy ligands, above and below the interlamellar space, to a three-dimensional framework with oval channels (Figure 4c).

Compound **3** was prepared from the hydrothermal reaction of $Na_2MoO_4{\cdot}2H_2O$, $CuSO_4{\cdot}5H_2O$, 4,4′-bpy, and nicotinic acid (nic) in acidified water (pH = 2.44, which is adequate to produce β-$[Mo_8O_{26}]^{4-}$). The IR spectrum exhibits a series of bands in the 1639−1072 cm^{-1} range associated with 4,4′-bpy and nicotinic acid ligands and displays strong bands from 958 to 719 cm^{-1} attributed to ν(Mo═O) and ν(Mo−O−Mo). The Raman spectrum also exhibits complex band patterns in the ranges of 1621−1037 and 967−784 cm^{-1} ascribed to the 4,4′-bpy

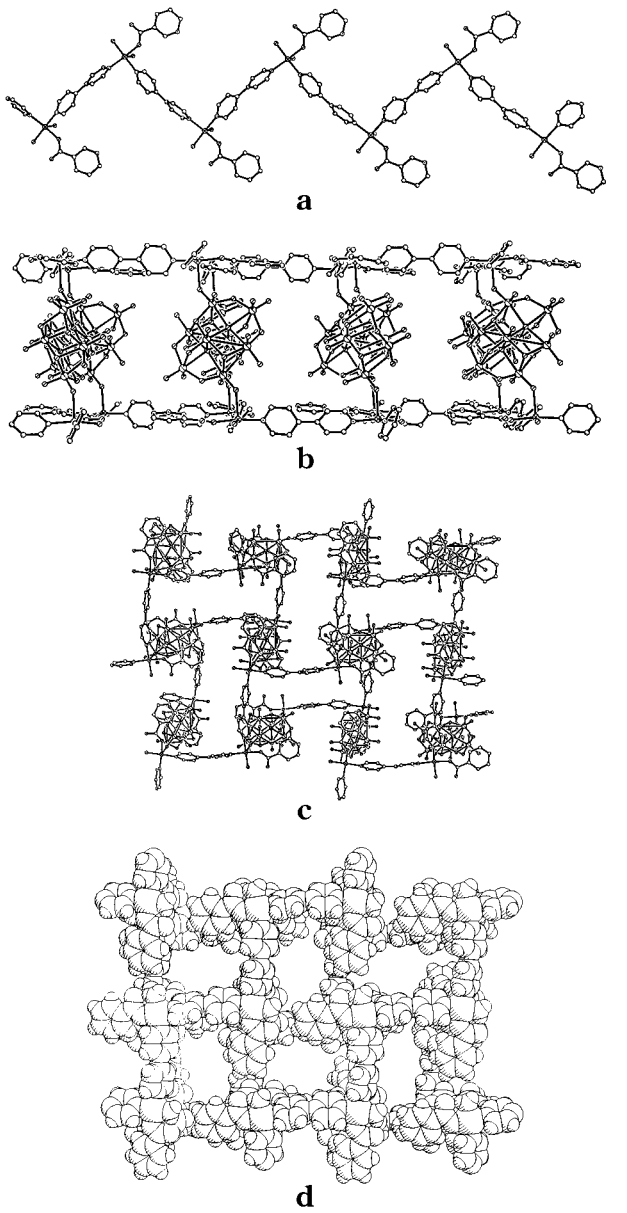

Figure 5. (a) View of the zigzag chains of $\{CuO_3N_2\}$ square pyramids linked by bidentate 4,4′-bpy ligands. (b) View of $[Cu(4,4\text{-bipy})(nic)(H_2O)]^{2+}$ chains linked by $[Mo_8O_{26}]^{4-}$ units to a sandwich-like layer (for clarity nicotinic acids are omitted). (c) Side view of **3** with rectangular cavities. (d) Space-filling view of the open-framework motif.

and nicotinic acid ligands and ν(Mo═O) or ν(Mo−O−Mo), respectively. The structure of **3** can be described as $[Cu(4,4'\text{-bpy})(nic)(H_2O)]_n^{2n+}$. One-dimensional zigzag chains are linked by $[Mo_8O_{26}]^{4-}$ cluster anions to form a sandwich-like layer. As shown in Figure 5b, the medium "layer" is the inorganic layer formed by β-$[Mo_8O_{26}]^{4-}$, while two covered "sheets" are five-coordinated Cu^{II} zigzag chains. The molybdenum core consists of edge-shared $\{MoO_6\}$ octahedra in the compact β-octamolybdate geometry.[18] The zigzag cationic chain $[Cu(4,4'\text{-bpy})(nic)(H_2O)]_n^{2n+}$ is formed by $\{CuO_3N_2\}$ square pyramids linked by bidentate 4,4′-bpy groups. Each Cu^{II} site is coordinated by two nitrogen donors from two 4,4′-bpy ligands (Cu−N = 1.995(4) and 1.996(4)

(18) Inoue, M.; Yamase, T. *Bull. Chem. Soc. Jpn.* **1995**, *68*, 3055, and references therein.

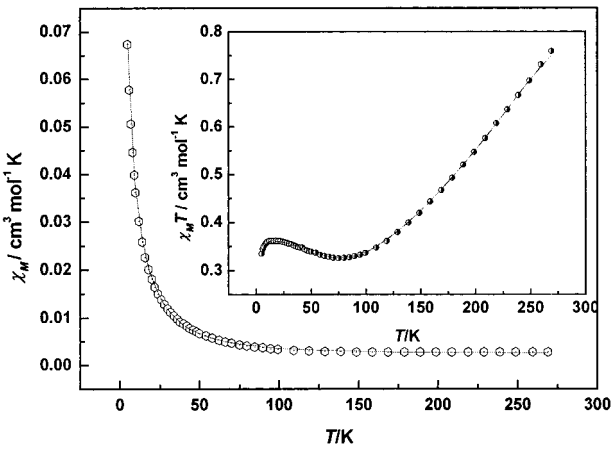

Figure 6. Plot of χ_M vs T for **3**. The insert shows the $\chi_M T$ vs T plots for compound **3** (solid lines represent the theoretical fits).

Å) in a cis pattern, one terminal aqua ligand (Cu−O = 1.930(5) Å), one terminal oxo group from the molybdate subunit (Cu−O = 2.276(4) Å), and one carboxylate group of nicotinic acid (Cu−O = 1.958(4) Å). Because the 4,4′-bpy groups occupy cis positions on the Cu^{II} sites, each $[Cu(4,4'\text{-bpy})(nic)(H_2O)]_n^{2n+}$ chain has a fold of about 90° at each Cu atom (Figure 5a). Interestingly, each nicotinic acid is coordinated to the Cu^{II} center only via its one carboxylate group, adopted as a monodentate ligand.

The most interesting structural feature of **3**, however, is that the $[Cu(4,4'\text{-bpy})(nic)(H_2O)]_n^{2n+}$ chains stack parallel to each other face to face in a staggered manner and then are joined together by β-$[Mo_8O_{26}]^{4-}$ units into the above-mentioned sandwich layer structure (Figure 5b). Unlike many previous reported cases, in complex **3**, β-$[Mo_8O_{26}]^{4-}$ anions link $[Cu(4,4'\text{-bpy})(nic)(H_2O)]_n^{2n+}$ chains through covalent bonding of a terminal oxo group of Mo centers to Cu^{II} sites to form rectangular cavities with dimensions of about 11.015 × 19.018 Å. Each cavity, in a two-dimensional flat brick wall-like layer structure, is perpendicular to its neighboring cavity, resulting in a beautiful mosaic layer (Figure 5c,d).

3.2. ESR and Magnetic Properties for 3. The powder ESR spectrum recorded at room temperature (293 K) for compound **3** shows a two-line pattern and gives $g_{\|} = 2.1257$ and $g_{\perp} = 2.0540$ with hyperfine constant $A_{\|} = 115.6$ G, which meet the values as expected for copper(II) ions with square-pyramidal geometries and $d_{x^2-y^2}$ electronic configurations.[19] Similarly, at 77 K, we get $g_{\|} = 2.1269$ and $g_{\perp} = 2.0555$ with $A_{\|} = 112.2$ G, which are almost constant compared with the results at room temperature.

The powder magnetic susceptibility of compound **3** has been studied. The variation of the molar magnetic susceptibility χ_M was investigated for compound **3** in the temperature range from 5.0 to 269 K in a 10 kG applied field. Figure 6 shows the magnetic behavior of **3** in the form of $\chi_M T$ vs T and χ_M vs T plots. At 269.0 K, the $\chi_M T$ value is 0.759 emu·K·mol^{-1} per dimer, which corresponds well with the value expected for two uncoupled $S = {}^1/_2$ spins (0.75 emu·K·mol^{-1} for $g = 2.0$). $\chi_M T$ decreases rapidly when lowering the temperature down to 75.0 K, where it displays a minimum (0.326 emu·K·mol^{-1}). Below 75.0 K, the $\chi_M T$ value of the product increases and exhibits a maximum (0.362 emu·K·mol^{-1}) at 16.0 K. Upon cooling to 5.0 K, the $\chi_M T$ values decrease gradually to 0.335 emu·K·mol^{-1}, indicating the presence of a magnetic impurity. To evaluate the superexchange coupling constants in such a magnetic system, the classical spin model developed by Fisher[20] and corrected for interchain coupling (eq 1) was used. In this case, J_1 is the intrachain exchange constant (transferred by 4,4′-bpy), J_2 is the interchain coupling constant (transferred by octamolybdate), and z is the number of interacting neighbors.

$$\chi_{\text{Mchain}} = Ng^2\beta^2S(S+1)/(3kT)(1+u)/(1-u) \quad (1a)$$

$$u = \coth[J_1S(S+1)/kT] - [kT/J_1S(S+1)] \quad (1b)$$

$$\chi_M = \chi_{\text{Mchain}}/(1 - 2zJ_2\chi_{\text{Mchain}}/Ng^2\beta^2) \quad (1c)$$

$$R = \sum[(\chi_M)_{\text{obsd}} - (\chi_M)_{\text{calcd}}]^2/\sum[(\chi_M)_{\text{obsd}}]^2 \quad (1d)$$

Least-squares fitting of all experimental data in the range of 5.0−269.0 K (solid line shown in Figure 6) leads to the following parameters: $J_1 = -4.63$ cm^{-1}, $J_2 = -1.82$ cm^{-1}, $g = 1.94$, and agreement factor $R = 3.447 \times 10^{-7}$. These results suggest the existence of weak antiferromagnetic interactions between the copper(II) intrachain atoms (J_1) and between adjacent chains (J_2). By a comparison of the framework and the magnetic behavior, the small negative superexchange constant J_1 and J_2 values imply that the exchange interaction through 4,4′-bpy and octamolybdate is weak. This result suggests that the distances between copper(II) atoms linked by 4,4′-bpy and octamolybdate are too long to form any strong interactions.

4. Conclusions

The discussions of **1**−**3** demonstrate that the acidity/basicity values have a crucial influence on the formation of products derived from hydrothermal media. For **3**, because the nic ligand is directly coordinated to the copper atom through a carboxylate group, it may also play important role in the construction of the interesting framework. In our case, the pH value influences not only the concentration of $\{MoO_x\}$ polyhedra and the oxidation state of the copper atom but also the organization of organic ligands, molybdenum(VI) oxides, and second transition metals in the formation of the products. On the other hand, different coordination environments of the "secondary" metal and organic ligand have an important impact on the structures of the products as well. It seems that organic ligands and inorganic oxide units can act as templates for each other. If the pH values in the hydrothermal syntheses have been properly controlled, inorganic oxide units and organic ligands can "work" together very well to produce interesting compounds with distinctive frameworks. It is certainly optimistic that more and more interesting new materials of this type with special architectures and useful properties will be obtained and well studied. As for **3**,

(19) *Magnetic Molecular Materials*; Gatteschi, D., Kahn, O., Miller, J. S., Palacio, F., Eds.; NATO ASI Series E198; Kluwer Academic Publishers: Dordrecht, The Netherlands, 1991.

(20) Fisher, M. E. *Am. J. Phys.* **1964**, *32*, 343.

the weak antiferromagnetic coupling among copper(II) atoms is transferred through 4,4′-bpy and octamolybdate.

Acknowledgment. This work was supported by the State Education Ministry, the State Personal Ministry, National Natural Science Foundation of China (20073048), NSF of Fujian, and the Chinese Academy of Sciences.

CM011725K